

Implications of JLA data for k -essence model of dark energy with given equation of state

Abhijit Bandyopadhyay¹ and Anirban Chatterjee²

Department of Physics
Ramakrishna Mission Vivekananda Educational and Research Institute
Belur Math, Howrah 711202, India

Abstract

We investigated implications of recently released ‘Joint Light-curve Analysis’ (JLA) supernova Ia (SNe Ia) data for dark energy models with time varying equation of state of dark energy, usually expressed as $w(z)$ in terms of variation with corresponding redshift z . From a comprehensive analysis of the JLA data, we obtain the observational constraints on the different functional forms of $w(z)$, corresponding to different varying dark energy models often considered in literature, *viz.* CPL, JBP, BA and Logarithmic models. The constraints are expressed in terms of parameters (w_a, w_b) appearing in the chosen functional form for $w(z)$, corresponding to each of the above mentioned models. Realising dark energy with varying equation of state in terms of a homogeneous scalar field ϕ , with its dynamics driven by a k -essence Lagrangian $L = VF(X)$ with a constant potential V and a dynamical term $F(X)$ with $X = (1/2)\nabla^\mu\phi\nabla_\mu\phi$ we reconstructed form of the function $F(X)$. This reconstruction has been performed for different varying dark energy models at best-fit values of parameters (w_a, w_b) obtained from analysis of JLA data. In the context of k -essence model, we also investigate the variation of adiabatic sound speed squared, $c_s^2(z)$, and obtained the domains in (w_a, w_b) parameter space corresponding to the physical bound $c_s^2 > 0$ implying stability of density perturbations.

1 Introduction

Measurement of redshift and luminosity distances for Type Ia Supernova (SNe Ia) events [1], [2], are instrumental in establishing the fact that the universe has undergone a transition from a phase of decelerated expansion to accelerated expansion during its late time phase of evolution. Other independent evidences in support of this fact come from the observations of Baryon Acoustic Oscillation ([3],[4],[5],[6],[7]), Cosmic Microwave Background radiations ([8],[9],[10],[11]) measurement of differential ages of the galaxies in GDDS, SPICES and VDSS surveys [12, 13, 14, 15] and studies of power spectrum of matter distributions of the universe. A general label attributed to the origin of this late time cosmic acceleration is ‘Dark Energy’ (DE). Besides, study of rotation curves of spiral galaxies [16], Bullet cluster [17], gravitational lensing [18], provide indirect evidence for existence of non-luminous matter in present universe. Such ‘matter’, labelled as ‘Dark Matter’ (DM) manifest its existence only through gravitational interactions. Measurements in satellite borne experiments - WMAP [19] and Planck [20] have established that, at present epoch, dark energy and dark matter comprise

¹Email: abhijit@rkmvu.ac.in

²Email: anirban.chatterjee@rkmvu.ac.in

around 96% of total energy density of the universe ($\sim 69\%$ dark energy and $\sim 27\%$ dark matter). Rest $\sim 4\%$ is contributed by baryonic matter with negligible contribution from radiations.

There exist diverse theoretical approaches aiming construction of different models for dark energy to explain the present day cosmic acceleration. These include the Λ -CDM model [21] which provides excellent agreement with the cosmological data. Here ‘CDM’ refers to Cold Dark Matter content of the universe and Λ , the cosmological constant, denotes vacuum energy density. Though this model provides a simple phenomenological solution, it is plagued with the problem of large disagreement between vacuum expectation value of energy momentum tensor and observed value of dark energy density (fine tuning problem). This motivates investigation of alternative models of dark energy. One of the key features of a class of such models, called varying dark energy models, is time varying equation of state $w = p/\rho$ (ρ is the energy density and p the pressure of dark energy) of dark energy which is usually expressed in terms of variation of w with redshift z (in Λ -CDM model $w = -1$, constant). The redshift dependence of the EOS parameter $w(z)$, in the context of the varying DE models may be constrained from the observational data. The starting point for dealing with the issue of variations of the EOS parameter $w(z)$ is to consider diverse functional forms of $w(z; w_a, w_b)$ each involving a small number of parameters (denoted in the text by symbols w_a, w_b). The observational constraints on the z -dependence of w may then be realised in terms of constraints on the parameters (w_a, w_b) for each different functional forms of $w(z; w_a, w_b)$ considered. In this work we have performed a comprehensive analysis of ‘Joint Light-curve Analysis’ (JLA) data ([22],[23],[24]) to obtain constraints on different functional forms of $w(z)$ often used in literature in the context of varying dark energy models ([25],[26],[27],[28],[29],[30],[31],[32],[33],[34],[35],[36] and references there in). As benchmark we have chosen four such models *viz.* CPL[25], JBP[29],[30], BA[31],[32] and and Logarithmic model [33], and for each model we presented the values of the parameters (w_a, w_b) those fit best the observational data from JLA and also shown the regions in this parameter space at different confidence limits allowed from observational data.

Dark energy with varying equation of state may be realised theoretically in terms of dynamics of a scalar field (ϕ). One class of such scalar field models, called ‘Quintessence’, is described in terms of standard canonical Lagrangian of the form $L = X - V(\phi)$ where $X = \frac{1}{2}\nabla_\mu\phi\nabla_\mu\phi$ is the kinetic term. There also exist alternative class of models involving Lagrangians with non-canonical kinetic terms as $L = V(\phi)F(X)$, where $F(X)$ is a function of X . Such models, called k -essence models, have interesting phenomenological consequences different from those of quintessence models. Another motivation for considering k -essence scalar fields is that they appear naturally in low energy effective string theory. Such theories with non-canonical kinetic terms was first proposed by Born and Infeld to get rid of the infinite self-energy of the electrons [37] and were also investigated by Heisenberg in the context of cosmic ray physics [38] and meson production [39]. In this work, we consider dark energy represented in terms of a homogeneous scalar field $\phi \equiv \phi(t)$ whose dynamics is driven by a k -essence Lagrangian $L = VF(X)$ with a constant potential V . The constancy of the potential ensures existence of a scaling relation, $XF_X^2 = Ca^{-6}$ ($C = \text{constant}$), in a Friedmann-Lemaitre-Robertson-Walker (FLRW) background space-time with scale factor a . We exploited the scaling relation and observational constraints on the parameters w_a, w_b , to reconstruct the forms of the function $F(X)$ for the different varying dark energy models.

In the context of k -essence model, we also investigate the adiabatic sound speed squared (c_s^2) [40] - the quantity relevant for the growth of small fluctuations in the background energy density. Imaginary value of the sound speed ($c_s^2 < 0$) implies instability of density perturbations. Also from causality, it requires the speed of propagation of density perturbations not to exceed the speed of light ($c_s^2 < 1$). However, it was pointed out in [41, 42, 43] that in k -essence theories superluminal propagation of perturbations on classical backgrounds is admissible and no causal paradoxes arise. This implies the condition $c_s^2 > 0$ would be enough to represent the physical bound in the context of k -essence theories. For each of the varying dark energy models considered here, we find z -dependence of c_s^2 at best-fit values of parameters w_a, w_b obtained from analysis of JLA data. This has been found over the entire redshift range $0 < z < 1.3$ accessible in SNe Ia observations corresponding to the JLA data. We note that at the best-fit, c_s^2 is not always within its physical bound ($c_s^2 > 0$) for all values of z in the above mentioned range. For each of the varying DE models, we have found the regions in $w_a - w_b$ parameter space for which the physical bound $c_s^2 > 0$ is satisfied for the entire range of values of z in JLA data. The best-fit values of parameters (w_a, w_b) for each model obtained from analysis of the observational data are found to lie outside this domain corresponding to the bound $c_s^2 > 0$ (and also to $0 < c_s^2 < 1$) implying that observational data allow values of parameters (w_a, w_b), for which the physical bound on c_s^2 is respected, only at higher confidence limits. For example, for BA and Logarithmic models the values of parameters (w_a, w_b) corresponding to $0 < c_s^2(z) < 1$ for all z is allowed from observational data only beyond $\sim 2\sigma$ confidence limits. It is allowed only at 3σ and beyond for CPL model and even at larger confidence limits for JBP model. For each of the models we have found the point in $w_a - w_b$ parameter space which belongs to the domain for which $0 < c_s^2 < 1$ for all z and is maximally favoured from observational data. The form of the k -essence Lagrangian density $F(X)$ are also reconstructed at these points.

The paper is organised as follows. In Sec. 2 we describe the methodology of analysis of the observational data and provide a brief description of the different data sets used in our analysis. In Sec. 3 we discussed different models of dark energy with varying equation of state and their realisations in terms of kessence scalar field models. In this context we also discussed relevance of investigating variations of the adiabatic sound speed squared. The methodology of obtaining form of the Lagrangian density $L = VF(X)$ for k -essence models are also described. In Sec. 4 we discussed the results on the variation of c_s^2 , form of the function $F(X)$ obtained from the analysis of the data. The conclusions are presented in Sec. 5.

2 Methodology of Analysis of Observational Data

Measurement of luminosity distances and redshift of type Ia supernovae (SNe Ia) are instrumental in probing nature of dark energy. There exist several systematic and dedicated measurements of SNe Ia events. There are different supernova surveys in different domains of redshift (z). High redshift projects ($z \sim 1$) include Supernova Legacy Survey (SNLS) ([44],[45]), the ESSENCE project [46], the Pan-STARRS survey ([47],[48],[49],[50]). The SDSS-II supernova surveys ([51],[52],[53], [54],[55]) probe the redshift regime $0.05 < z < 0.4$. The surveys in the small redshift domain ($z > 0.1$) are the Harvard-Smithsonian Center for Astrophysics survey [56], the Carnegie Supernova Project ([57],[58],[59]) the Lick Observatory

Supernova Search [60] and the Nearby Supernova Factory [61]. Other different compilations of SNe Ia data may also be found in ([62],[63],[64]) and references in [46]. Nearly one thousand of SNe Ia events were discovered in all these surveys.

The recently released ‘‘Joint Light-curve Analysis’’ (JLA) data ([22],[23],[24]) is a compilation of several low, intermediate and high redshift samples including data from the full three years of the SDSS survey, first three seasons of the five-year SNLS survey and 14 very high redshift $0.7 < z < 1.4$ SNe Ia from space-based observations with the HST [12]. This data set contains 740 spectroscopically confirmed SNe Ia events with high-quality light curves.

In this section we describe the methodology of analysis of JLA data to obtain bounds on equation of state parameter w of dark energy. There exist diverse statistical techniques for analysis of JLA data. Some of these methods are discussed in detail in ([33],[65],[66],[67],[68]). However, we take the χ^2 function corresponding to JLA data as [23, 24]

$$\chi_{\text{SN}}^2 = \sum_{i,j} \left(\mu_{\text{obs}}^{(i)} - \mu_{\text{th}}^{(i)} \right) (\Sigma^{-1})_{ij} \left(\mu_{\text{obs}}^{(j)} - \mu_{\text{th}}^{(j)} \right) \quad (1)$$

where values of the dummy indices i, j run from 1 to 740 corresponding to the 740 SNe Ia events contained in the JLA data set [23]. $\mu_{\text{th}}^{(i)}$ stands for the theoretical expression for distance modulus in a flat FRW spacetime background for the i^{th} entry of the JLA data set and is given by

$$\mu_{\text{th}}^{(i)} = 5 \log \left[\frac{d_L(z_{\text{hel}}, z_{\text{CMB}})}{\text{Mpc}} \right] + 25 \quad (2)$$

where

$$d_L(z_{\text{hel}}, z_{\text{CMB}}) = (1 + z_{\text{hel}})r(z_{\text{CMB}}) \quad \text{with} \quad r(z) = cH_0^{-1} \int_0^z \frac{dz'}{E(z')}. \quad (3)$$

d_L is the luminosity distance, $r(z)$ is the comoving distance to an object corresponding to a redshift z . z_{CMB} and z_{hel} are SNe Ia redshifts in CMB rest frame and in heliocentric frame respectively. c is the speed of light and H_0 is the value of Hubble parameter at present epoch. The function $E(z)$ in Eq. (3) is the reduced Hubble parameter given by

$$E(z) \equiv \frac{H(z)}{H_0} = \left\{ \Omega_r^{(0)}(1+z)^4 + \Omega_m^{(0)}(1+z)^3 + \Omega_{de}^{(0)} \exp \left[3 \int_0^z dz' \frac{1+w(z')}{1+z'} \right] \right\}^{1/2} \quad (4)$$

where $\Omega_r^{(0)}$, $\Omega_m^{(0)}$ and $\Omega_{de}^{(0)}$ are the values of fractional energy density contributions from radiation, matter and dark energy respectively at present epoch.

$\mu_{\text{obs}}^{(i)}$ is the observed value of distance modulus at a redshift z_i corresponding to i^{th} entry of the JLA data set. This is expressed through the following empirical relation as

$$\mu_{\text{obs}}^{(i)} = m_B(z_i) - M_B + \alpha X_1(z_i) - \beta C(z_i) \quad (5)$$

where $m_B(z_i)$ is the observed value of peak magnitude, $X_1(z_i)$ denotes time stretching of the light-curve and $C(z_i)$ is the supernova ‘color’ at maximum brightness. M_B is the absolute

magnitude which we take fixed at $M = -19$ for our work and α, β are nuisance parameters. Σ is the total covariant matrix given in terms of statistical and systematic uncertainties as

$$\begin{aligned} \Sigma_{ij} = & \delta_{ij} \left[(\sigma_z^2)_i + (\sigma_{\text{int}}^2)_i + (\sigma_{\text{lensing}}^2)_i + (\sigma_{m_B}^2)_i + \alpha^2 (\sigma_{X_1}^2)_i + \beta^2 (\sigma_C^2)_i \right. \\ & \left. + 2\alpha (\Sigma_{m_B, X_1})_i - 2\beta (\Sigma_{m_B, C})_i - 2\alpha\beta (\Sigma_{X_1, C})_i \right] \\ & + \left[(V_0)_{ij} + \alpha^2 (V_a)_{ij} + \beta^2 (V_b)_{ij} + 2\alpha (V_{0a})_{ij} - 2\beta (V_{0b})_{ij} - 2\alpha\beta (V_{ab})_{ij} \right] \end{aligned} \quad (6)$$

The terms in the first two lines of Eq. (6) represent the diagonal part of the covariance matrix. These include Statistical uncertainties in redshifts (σ_z^2), in SNe IA magnitudes (owing to intrinsic variation (σ_{int}^2) and gravitational lensing ($\sigma_{\text{lensing}}^2$), in m_B ($\sigma_{m_B}^2$), X_1 ($\sigma_{X_1}^2$) and Color (σ_C^2) and covariances between them ($\Sigma_{m_B, X_1}, \Sigma_{m_B, C}, \Sigma_{X_1, C}$) in each bin. The terms in last line of Eq. (6) involving matrices ($V_0, V_a, V_b, V_{0a}, V_{0b}, V_{ab}$) correspond to the off-diagonal part of the covariance matrix originating from statistical and systematic uncertainties. All these matrices are given by JLA group and are extensively discussed in [23, 24].

We note from Eqs. (2), (3) and (4) that evaluation of $\mu_{\text{th}}^{(i)}$ requires values of parameters $\Omega_r^{(0)}$, $\Omega_m^{(0)}$ and $\Omega_{de}^{(0)}$ and knowledge of functional form of equation of state (EOS) $w(z)$ of dark energy. Since in a spatially flat universe $\Omega_r^{(0)} + \Omega_m^{(0)} + \Omega_{de}^{(0)} = 1$, neglecting the value of fractional density contribution of radiation at present epoch with respect to those from other components, we have $\Omega_{de}^{(0)} \approx 1 - \Omega_m^{(0)}$. We may also choose different functional form of dark energy EOS which we denote by a general symbol $w(z; w_a, w_b, \dots)$, where w_a, w_b, \dots denote the parameters of the chosen functional dependence. On the other hand, the nuisance parameters α and β enter in the expression for $\mu_{\text{obs}}^{(i)0}$ (Eq. (5)) and the covariance matrix as well (Eq. (6)). The χ_{SN}^2 function, in Eq. (1), are minimised with respect to the parameters $w_a, w_b, \Omega_m^0, \alpha, \beta$. The (best-fit) values of these parameters corresponding to the minimum value of χ^2 for different chosen models of dark energy EOS are presented in Sec 4.

Besides SNe Ia data, compilation of measurements of differential ages of the galaxies in GDDS, SPICES and VDSS surveys gives measured values of Hubble parameter at 15 different redshift values [12, 13, 14, 15] The χ^2 function for the analysis of this observational Hubble data (OHD) may be defined as

$$\chi_{\text{OHD}}^2 = \sum_{i=1}^{15} \left[\frac{H(w_a, w_b, \Omega_m^{(0)}; z_i) - H_{\text{obs}}(z_i)}{\Sigma_i} \right]^2 \quad (7)$$

where $H_{\text{obs}}(z_i)$ is the Observed value of the Hubble parameter at redshift z_i with 1σ uncertainty Σ_i and $H(w_a, w_b, \Omega_m^{(0)}; z_i)$ is its theoretical value evaluated by multiplying $E(z)$ in Eq. (4) by H_0 . Also, observation of Baryon Acoustic Oscillations (BAO) in Sloan Digital Sky Survey (SDSS) provide measurement of correlation function of the large sample of luminous red galaxies. Using the detected acoustic peak value of a dimensionless standard ruler $A(z_1)$ corresponding to a typical redshift $z_1 = 0.35$ may be determined. The theoretical expression for the quantity $A(z_1)$ is given by

$$A(w_a, w_b, \Omega_m^{(0)}; z_1) = \frac{\sqrt{\Omega_m^{(0)}}}{E^{1/3}(z_1)} \left[\frac{1}{z_1} \int_0^{z_1} \frac{dz}{E(z)} \right]^{2/3} \quad (8)$$

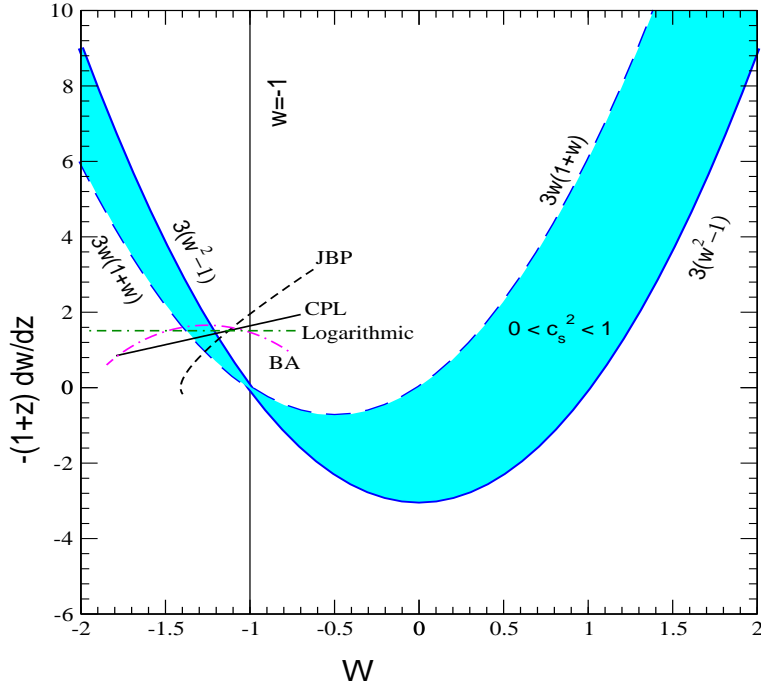


Figure 1: Pictorial representations of the conditions for $c_s^2 > 0$ and $c_s^2 < 1$ in the parameter space spanned by w and $-(1+z)dw/dz$ (See Eqs. (24) and (25)). For $w < -1$, the region lying above the dotted line ($3w(1+w)$) and for $w > -1$ region lying below the dotted line corresponds to $c_s^2 > 0$. The shaded region corresponds to the bound $0 < c_s^2 < 1$. The curves at the best-fit (w_a, w_b) points corresponding to different parametrisations of $w(z)$ in different varying dark energy models are also shown.

where the parameters $w_a, w_b, \Omega_m^{(0)}$ enter in the above expression through the function $E(z)$ (Eq. (4)). The observed value of the standard ruler $A_{\text{obs}} \pm \Delta A$ is 0.469 ± 0.017 and the χ^2 -function for the BAO data is taken as

$$\chi_{\text{BAO}}^2 = \frac{[A(w_a, w_b, \Omega_m^{(0)}; z_1) - A_{\text{obs}}]^2}{(\Delta A)^2} \quad (9)$$

To illustrate the impact of the Observational Hubble data and BAO data we have performed a combined analysis of SNe IA, OHD and BAO data by minimising the total χ^2 function

$$\chi^2 \equiv \chi_{\text{SN}}^2 + \chi_{\text{OHD}}^2 + \chi_{\text{BAO}}^2 \quad (10)$$

with respect to the parameter set $(w_a, w_b, \Omega_m^0, \alpha, \beta)$. Results of the analysis are presented in Sec. 4.

3 k -essence and Varying Dark energy

In this work we investigate realisation of dark energy with varying equation of state in terms of k -essence scalar field models. We assume dark energy represented in terms of a homogeneous

scalar field whose dynamics is driven by a k -essence Lagrangian with constant potential. In this context, we give below a brief outline of basic equations of k -essence model *i.e.*

$$L = V(\phi)F(X) = p \quad (11)$$

$$\rho = V(\phi)(2XF_X - F) \quad (12)$$

where L is the k -essence Lagrangian, ρ and p respectively represent energy density and pressure of dark energy. $F(X)$ is a function of X , where $X = \frac{1}{2}\nabla_\mu\phi\nabla^\mu\phi$, $F_X \equiv dF/dX$ and $V(\phi)$ represents the potential. In a flat FLRW spacetime background, ρ and p are related by the continuity equation

$$\dot{\rho} + 3H(\rho + p) = 0, \quad (13)$$

where $H = \dot{a}/a$ is the Hubble constant and $a(t)$ is the scale factor. For a homogeneous scalar field ϕ , in a flat FLRW spacetime background, we have $X = \frac{1}{2}\dot{\phi}^2$. We consider k -essence models with constant potential $V(\phi) = V$ which ensures existence of scaling relation [69, 70]

$$XF_X^2 = Ca^{-6} \quad (14)$$

where C is a constant. The equation of state of dark energy represented by k -essence field is given by

$$w = \frac{p}{\rho} = \frac{F}{2XF_X - F} \quad (15)$$

The issue of causality in the context of k -essence scalar field theories with Lorentz invariant action of the form $S = \int d^4x\sqrt{-g}L(\phi, X)$ where g is the determinant of the FRW metric considered here and L is the Lagrangian in Eq. (11) has been discussed in detail in [43, 71]. Variation of the action with respect to the scalar field gives the equation of motion of the scalar field ϕ as

$$G^{\mu\nu}\nabla_\mu\nabla_\nu\phi + 2X\frac{\partial}{\partial X}\left(\frac{\partial L}{\partial\phi}\right) - \frac{\partial L}{\partial\phi} = 0 \quad (16)$$

where, the effective metric $G^{\mu\nu} \equiv L_X g^{\mu\nu} + L_{XX}\nabla^\mu\phi\nabla^\nu\phi$ with L_X and L_{XX} denoting $\partial L/\partial X$ and $\partial^2 L/\partial X^2$ respectively, has a Lorentzian structure and describes the time evolution of the system if the following condition is satisfied [43, 72, 73, 74]

$$1 + 2X\frac{L_{XX}}{L_X} > 0 \quad (17)$$

Now introducing c_s^2 as

$$c_s^2 \equiv \left[1 + 2X\frac{L_{XX}}{L_X}\right]^{-1} \quad (18)$$

it has been shown in [75], that for $X(= \frac{1}{2}\dot{\phi}^2, \text{ in our case}) > 0$, the quantity c_s^2 plays the role of sound speed squared for propagation of small perturbations. However, in the context of spatially flat FRW universe, with small perturbations, neglecting vector perturbations which decay as a^{-2} , the metric may be written as

$$ds^2 = (1 + 2\Phi)dt^2 - a^2(t)[(1 - 2\Phi)\delta_{ij} + h_{ij}]dx^i dx^j \quad (19)$$

where Φ (the gravitational Newtonian potential) is the scalar perturbation and h_{ij} is traceless transverse perturbations. From the standard results of cosmological perturbation theory [75, 76, 77], it follows that perturbations in the k-essence field $\delta\phi$, which are gauge invariant are connected with the scalar metric perturbations and the dynamics of cosmological perturbation may be described by the action of the form

$$S_c = \frac{1}{2} \int d^3x d\eta \left[\left(\frac{dv}{d\eta} \right)^2 - c_s^2 (\nabla v)^2 - m_c^2 v^2 \right] \quad (20)$$

where $\eta \equiv \int dt/a(t)$ is the conformal time, $v \equiv \sqrt{\frac{d\rho}{dX}} a (\delta\phi + \frac{1}{\mathcal{H}} \frac{d\phi}{d\eta} \Phi)$, $\mathcal{H} = (1/a)(da/d\eta)$, $m_c^2 \equiv -(1/z)(d^2z/d\eta^2)$ with $z \equiv \sqrt{\frac{d\rho}{dX}} \frac{a}{\mathcal{H}} \frac{d\phi}{d\eta}$ and the quantity c_s^2 representing sound speed squared for propagation of small perturbations in Eq. (20) is given by

$$c_s^2 = \frac{dp/dX}{d\rho/dX} \quad (21)$$

A derivation for the above formula from an effective hydrodynamical description of the system is also obtained in [71].

Therefore, for the classical solutions $F(X)$ of the scaling relation Eq. (14) to be stable against small perturbations of the background energy density, the square of adiabatic sound speed should be positive ($c_s^2 > 0$). On the other hand, causality arguments require that this speed of propagation small perturbations of the background should not exceed the speed of light, implying $c_s^2 < 1$ [78, 79, 80]. In the context of k -essence model, using Eqs. (11) and (12) in (21) we have

$$c_s^2 = \frac{F_X}{2X F_{XX} + F_X} \quad (22)$$

Using $1/a = 1 + z$ (where z is the redshift and value of scale factor a at present epoch is normalised to unity) in $H = \dot{a}/a$ we have $dt = -dz/(1+z)H$. Exploiting this result and transforming time dependences of ρ , p and w to their z -dependences in Eq. (13) we may also express the sound speed squared as a function of redshift z as

$$c_s^2 = \frac{3w(1+w) + (1+z)dw/dz}{3(1+w)} \quad (23)$$

We note from Eq. (23) that the bound $c_s^2 > 0$ corresponds to

$$\begin{aligned} \text{either} & \quad -(1+z)dw/dz < 3w(1+w), w > -1 \\ \text{or} & \quad -(1+z)dw/dz > 3w(1+w), w < -1 \end{aligned} \quad (24)$$

and the bound $c_s^2 < 1$ corresponds to

$$\begin{aligned} \text{either} & \quad -(1+z)dw/dz > 3(w^2 - 1), w > -1 \\ \text{or} & \quad -(1+z)dw/dz < 3(w^2 - 1), w < -1 \end{aligned} \quad (25)$$

Whether the physical bound $c_s^2 > 0$ (or $0 < c_s^2 < 1$) is realised for any chosen functional form of equation of state $w(z)$ may be verified by checking the conditions given in Eq. (24)

Model	$w(w_a, w_b; z)$	$Y(z) \equiv \exp \left[3 \int_0^z dz' \frac{1+w(z')}{1+z'} \right]$
CPL [25]	$w_a + w_b \frac{z}{1+z}$	$(1+z)^{3(1+w_a+w_b)} \exp \left(\frac{-3w_a z}{1+z} \right)$
JBP [29],[30]	$w_a + \frac{w_b z}{(1+z)^2}$	$(1+z)^{3(1+w_a)} \exp \left(\frac{3w_b z^2}{2(1+z)^2} \right)$
BA [31],[32]	$w_a + \left(\frac{w_b z(1+z)}{1+z^2} \right)$	$(1+z)^{3(1+w_a)} (1+z^2)^{\frac{3w_b}{2}}$
Logarithmic [33]	$w_a + w_b \log(1+z)$	$(1+z)^{3(1+w_a + \frac{w_b}{2} \log(1+z))}$

Table 1: Functional forms of equation of state $w(z)$ of dark energy as used in different varying dark energy Models. Expressions for corresponding z -dependences of dark energy density, expressed through the function $Y(z)$ (Eq. ((26))) are also given.

(or Eqs. (24) and (25)). These conditions are pictorially demonstrated in Fig. 1 (see [78] for details) where we have studied effect of the conditions on the plane spanned by quantities w and $-(1+z)dw/dz$. The shaded region marked in the figure is bounded by two curves $-(1+z)dw/dz = 3w(1+w)$ (dashed line) and $-(1+z)dw/dz = 3(w^2 - 1)$ (solid line). We have also shown the $w = -1$ line in the plane. From Eq. (24) and (25) we see that $c_s^2 > 0$ corresponds to the region in the plane which is below the dashed line for $w > -1$ and above the dashed line for $w < -1$. The condition $c_s^2 < 1$, on the other hand, corresponds to the region lying above the solid line for $w > -1$ and below the solid line for $w < -1$. The shaded region, bounded between these two lines in the plane, therefore corresponds $0 < c_s^2 < 1$ for the entire range of values of z accessible in the observations considered here.

Variation in the dark energy density $\rho(z)$ may be expressed in terms of variation of dark energy equation of state $w(z)$. Expression for a general functional form of $w(z)$, in principle, involves infinite number of parameters. However, for a practical analysis its effective to express the functional dependence $w(z)$, in terms a small number of parameters and consider different forms of parametrizations of $w(z)$. We consider here 4 different models, often used in literature in the context of varying dark energy, *viz.* CPL[25], JBP[29],[30], BA([31],[32]) and Logarithmic model [33]. Each of the models uses a specific functional form of $w(z)$ expressed in terms of two parameters (w_a and w_b) and are listed in Table 1 where we have also given functional form of the quantity $Y(z) \equiv \exp \left[3 \int_0^z dz' \frac{1+w(z')}{1+z'} \right]$ which gives the z -dependence of the corresponding dark energy density $\rho(z)$ (see Eq. (26)). In the plane of Fig. 1, we have also shown the curves representing the different parametrisations of $w(z)$ for the best-fit values of parameters w_a and w_b obtained from the analysis of observational data (see Sec. 4).

We finally exploit the equations of k -essence models to reconstruct the form the function $F(X)$. Using Eq. (13) we express energy density as a function of redshift as

$$\rho = \rho^{(0)} Y(z), \quad \text{where } Y(z) = \exp \left[3 \int_0^z dz' \frac{1+w(z')}{1+z'} \right] \quad (26)$$

where $\rho^{(0)}$ corresponds to value of dark energy density at present epoch ($z = 0$). Using Eqs.

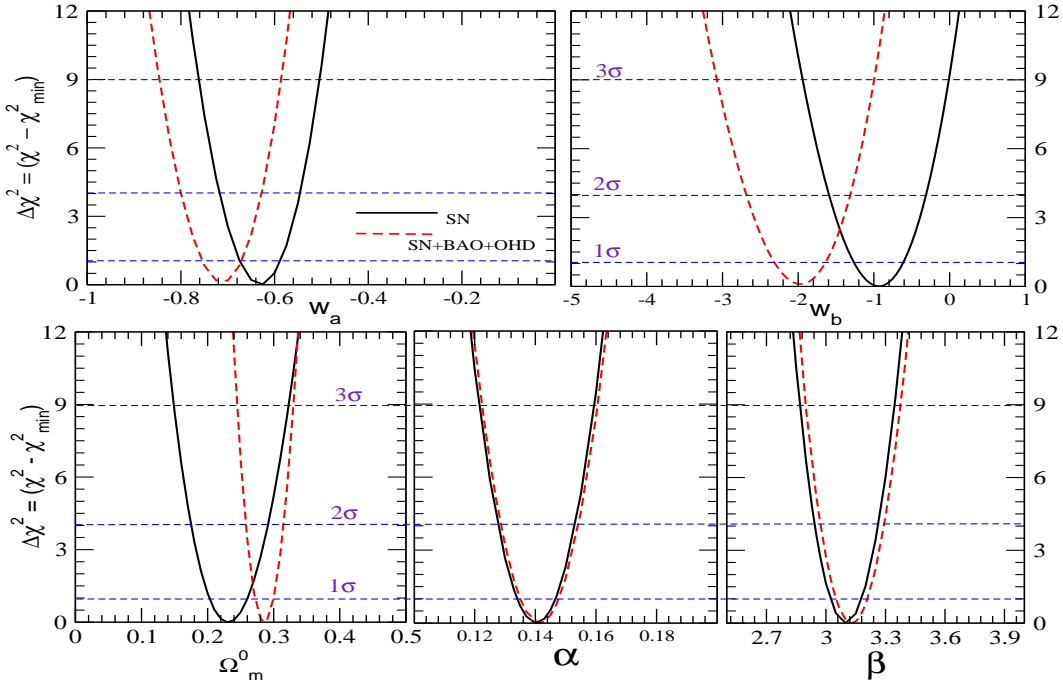


Figure 2: Plots of $\chi^2 - \chi_{\min}^2$ as a function of each individual parameters of the set (w_a , w_b , Ω_m^0 , α and β). The CPL parametrisation of $w(z)$ has been used. In each of the plots, depicting variation of χ^2 with one of the parameters at a time, values of the other parameters are kept fixed at their respective best-fit values as given in Tab. 2 (solid lines for best-fits of SNe Ia data alone and dotted lines for the best-fits from the combined analysis of SNe Ia, BAO and OHD). The values of $\Delta\chi^2$ viz. 1, 4 and 9, corresponding respectively to one parameter confidence levels of 1σ , 2σ and 3σ are shown by dotted horizontal lines.

(11), (12), (14) and (26) we obtain,

$$\left(\frac{4CV^2}{\rho(0)^2}\right)X = \frac{Y^2(z)(1+w(z))^2}{(1+z)^6} \quad (27)$$

Writing $p = \rho w$ in Eq. (11) and then using Eq. (26) we have,

$$\left(\frac{V}{\rho(0)}\right)F(X) = Y(z)w(z) \quad (28)$$

For a given form of the equation of state $w(z)$, the right hand sides of Eqs. (27) and (28) may be evaluated numerically at each z . Eliminating z from both the equations one may obtain the X -dependence of the function $F(X)$ corresponding to a given form of $w(z)$. The dependences of $F(X)$ on X obtained from the analysis of observational data are shown and described in Sec. 4.

4 Results of analysis of observed data

In this section we present the results of analysis of the observational data using the methodology described in Sec. 2. We investigate implications of the observations in the context of the

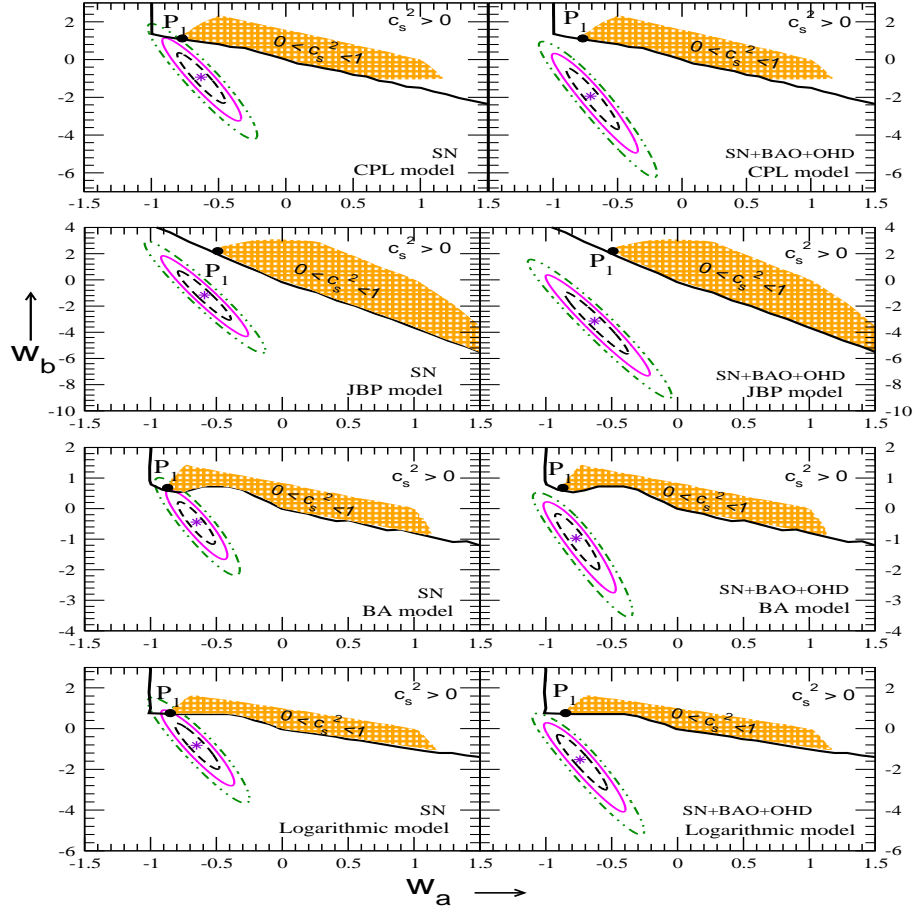


Figure 3: Regions of $w_a - w_b$ parameter space allowed at 1σ , 2σ and 3σ confidence limits from analysis of SNe Ia data (left panel) and SNe Ia + BAO + OHD (right panel). The results for 4 different types of parametrisations of $w(z)$ are shown in different rows. The corresponding best-fit point and the point P_1 are also shown (see text for details). The region above the black solid line corresponds to $c_s^2 > 0$. The shaded region in the figure corresponds to the bound $0 < c_s^2 < 1$.

varying dark energy models listed in Table 1. For each of the models we obtain the best-fit values of the parameters (w_a , w_b) along with their allowed domains at different confidence limits from the analysis. We perform analysis of SNe Ia data alone and also a combined analysis of data from SNe Ia, BAO and OHD (discussed in Sec. 2) where we freely vary the parameters w_a , w_b , Ω_m^0 , α and β to find their best-fit values (corresponding to minimum value of χ^2 in Eq. (10)). The obtained best-fit values of the above parameters for different models are presented in Table 2.

We also find the ranges of the individual parameters allowed at different confidence levels from the analysis of the observational data. To obtain this, we find the variation of χ^2 with each of the parameters of the set $\{w_a, w_b, \Omega_m^0, \alpha, \beta\}$ at a time, keeping values of all other parameters fixed at their respective best-fit values. The confidence interval for the single

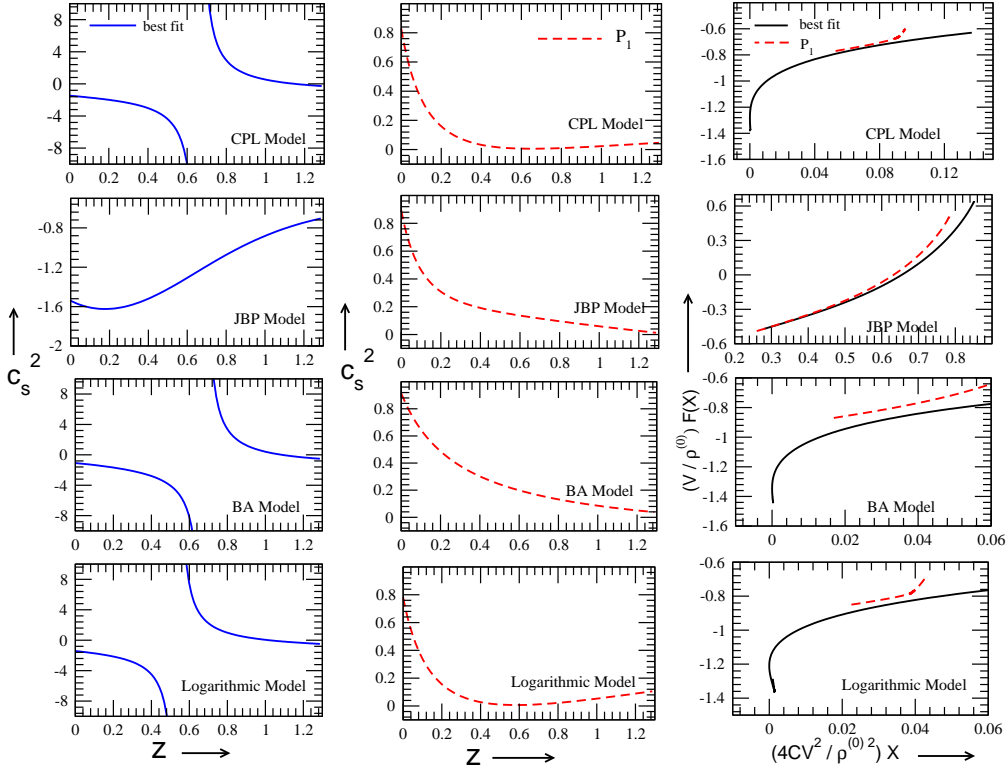


Figure 4: Plot of c_s^2 vs z for different parametrisations of $w(z)$ at best-fit (right panel) from SNe Ia data and at P_1 (middle panel) (see text for details). Corresponding plots of $F(X)$ vs X reconstructed at best-fit and P_1 are shown in right panel.

Data Set	Model	w_a	w_b	Ω_m^0	α	β	χ^2/DOF	Range of z	
								for which $0 < c_s^2 < 1$	$P_1(w_a, w_b)$
SNe Ia	CPL	-0.63	-0.93	0.23	0.14	3.1	685.42/735	0.93 - 1.15	(-0.77, 1.15)
	JBP	-0.59	-1.16	0.20	0.14	3.1	685.39/735	-	(-0.49, 2.22)
	BA	-0.65	-0.44	0.22	0.14	3.1	685.48/735	0.94 - 1.10	(-0.87, 0.65)
	Log.	-0.65	-0.82	0.24	0.14	3.1	685.44/735	0.79 - 1.01	(-0.85, 0.76)
SNe Ia + BAO + OHD	CPL	-0.71	-1.94	0.29	0.14	3.13	708.26/751	0.35 - 0.47	
	JBP	-0.63	-3.14	0.28	0.14	3.13	707.65/751	0.31 - 0.39	
	BA	-0.77	-0.97	0.29	0.14	3.13	708.86/751	0.45 - 0.53	
	Log.	-0.74	-1.52	0.29	0.14	3.13	708.56/751	0.38 - 0.51	

Table 2: Best-fit values of parameters for different models from analysis of SNe Ia data alone and SNe + BAO + OHD. The values of χ^2 (χ_{\min}^2) at the best-fit point per DOF (degrees of freedom) are also shown. The range of z for which the value of c_s^2 evaluated at best-fit lies between 0 and 1 are also shown. Last column shows the values of (w_a, w_b) corresponding to point P_1 (see text for details).

Data Set	Model	1σ & 3σ range of w_a	1σ & 3σ range of w_b	1σ & 3σ range of Ω_m^0	1σ & 3σ range of α	1σ & 3σ range of β
SNe Ia	CPL	[-0.67,-0.58] & [-0.76,-0.50]	[-1.25,-0.60] & [-1.95,0.01]	[0.20 ,0.26] & [0.15 ,0.32]	[0.13,0.15] & [0.12,0.16]	[0.24,0.25] & [0.23,0.26]
	JBP	[-0.63,-0.55] & [-0.70,-0.47]	[-1.51-0.77] & [-2.27,-0.05]	[0.17 ,0.23] & [0.12,0.30]		
	BA	[-0.69,-0.61] & [-0.77,-0.52]	[-0.64-0.23] & [-1.10,0.17]	[0.19 ,0.25] & [0.12,0.30]		
	Log.	[-0.69,-0.60] & [-0.78,-0.51]	[-1.12-0.48] & [-1.71,0.05]	[0.22,0.27] & [0.16,0.33]		
SNe Ia +BAO +OHD	CPL	[-0.75,-0.67] & [-0.84,-0.58]	[-2.3,-1.63] & [-3.07,-0.98]	[0.27 ,0.30] & [0.24 ,0.33]	[0.13 ,0.15] & [0.12 ,0.16]	[0.24,0.25] & [0.23,0.26]
	JBP	[-0.65,-0.58] & [-0.74,-0.49]	[-3.39,-2.6] & [-4.25,-1.82]	[0.27,0.30] & [0.24 ,0.33]		
	BA	[-0.82,-0.74] & [-0.91,-0.65]	[-1.24,-0.79] & [-1.80,-0.32]	[0.27 ,0.30] & [0.24 ,0.33]		
	Log.	[-0.78,-0.70] & [-0.87,-0.61]	[-1.84,-1.22] & [-2.53,-0.68]	[0.27 ,0.30] & [0.24 ,0.33]		

Table 3: 1σ and 3σ confidence limits of the each of the individual parameters of the set (w_a , w_b , Ω_m^0 , α and β) for different parametrisations of $w(z)$ (See text for details.)

parameter may then be obtained from the distribution of the function $\Delta\chi^2 \equiv \chi^2 - \chi_{\min}^2$ [81]. The range of values of the parameter for which $\Delta\chi^2 \leq 1$, $\Delta\chi^2 \leq 4$ and $\Delta\chi^2 \leq 9$ respectively correspond to 1σ (68.3% Confidence Level (C.L)), 2σ (95.4% C.L) and 3σ (99.73% C.L) [81] allowed intervals of the parameter. We have shown in Fig. 2 the nature of dependence of $\Delta\chi^2 \equiv \chi^2 - \chi_{\min}^2$ on each of the individual parameters. For demonstrative purpose, we have shown the plot for CPL model only. However, the obtained 1σ and 3σ ranges of the individual parameters for different models of parametrisations of $w(z)$, are given in Tab. 3.

For a comparative study of the different parametrisations of $w(z)$, we have also displayed the joint confidence region in the parameter space of w_a and w_b . To obtain this we keep the other parameters (ω_m^0 , α , β) at their respective best-fit values and obtain domains in $w_a - w_b$ parameter space for which evaluated values of χ^2 lie in the domain $\chi^2 = \chi_{\min}^2 + \Delta\chi^2$. The 1σ , 2σ and 3σ joint confidence region of two parameters (w_a and w_b) correspond to $\Delta\chi^2 < 2.30$, $\Delta\chi^2 < 6.17$ and $\Delta\chi^2 < 11.8$ respectively [81]. The obtained joint confidence regions in $w_a - w_b$ parameter space for the different $w(z)$ parametrisations are shown in Fig. 3. The corresponding best-fit points are also shown in the parameter space.

In the context of k -essence model of dark energy, we investigate, to what extent the condition $0 < c_s^2 < 1$ is favoured from observational data for different parametrisations of the dark energy equation of state $w(z)$. We used the different parametrisations of $w(z)$ in Eqs. (24) and (25) to find the range of values of the parameters w_a and w_b for which the condition $0 < c_s^2 < 1$ is satisfied for all z within the domain of observations. For each of the parametrisations of $w(z)$ mentioned in Table 1, this range is shown by a shaded region in $w_a - w_b$ plane

in Fig. 3. The regions corresponding to $c_s^2 > 0$ only are also shown for each model. We then observe that for all the models, the shaded region corresponding to $0 < c_s^2 < 1$ has no overlap with the region bounded by 1σ contour allowed from analysis of SNe Ia data alone. For BA and Logarithmic models the overlap is seen when one considers allowed ranges at and beyond $\sim 2\sigma$ confidence limits. This implies that the physical bound $0 < c_s^2 < 1$ for the entire range of values of z probed by the observed data considered here, is favoured from observational data (SNe Ia only) at and above $\sim 2\sigma$ confidence level if we consider parametrisations of $w(z)$ as in BA and Logarithmic models. For CPL parametrisation the physical bound is disfavoured below $\sim 3\sigma$ and with JBP its disfavoured upto even higher confidence limits. For all the different parametrisations of $w(z)$ the physical bound is disfavoured to a larger extent from a combined analysis of SNe Ia, BAO and OHD. In the $w_a - w_b$ parameter space shown in Fig. 3, we have also marked a point P_1 in the shaded region corresponding to $0 < c_s^2 < 1$, at which the value of χ^2 is closest to the value of χ_{\min}^2 for the corresponding model. Thus P_1 refers to the maximally favoured values of parameters w_a and w_b from observational data for which c_s^2 lies between 0 and 1 for all z values. The values of (w_a, w_b) corresponding to P_1 are shown in the last column of table 2.

At the best-fit values of parameters w_a and w_b obtained from the combined analyses of observational data from SNe Ia, BAO and OHD for different $w(z)$ parametrisations we have shown the variation of sound speed squared $c_s^2(z)$ with redshift z in left panel of Fig. 4. We see that at the best-fit values of the parameters the calculated value of c_s^2 lies within its physical bound $0 < c_s^2 < 1$ only for a very narrow range of values of z . These ranges are also shown in Table 2. The variation of c_s^2 at values of w_a, w_b corresponding to the point P_1 are shown for different models in the middle panel of Fig. 4. These correspond to a monotonous variation of c_s^2 with z within its physical bound $0 < c_s^2 < 1$ imposed by causality and stability.

In Sec. 3 we discussed the methodology to reconstruct the form of function $F(X)$ for different form of parametrisations of $w(z)$. We have shown in right panel of Fig. (4) the obtained dependences of $F(X)$ on X , for each of the models at the corresponding best-fit values of the parameters (w_a, w_b) . The Figure shows that for JBP model $F(X)$ has a monotonous dependence of X whereas for the other models (CPL, BA and Logarithmic) the function is double valued in a certain domain of X .

As discussed earlier, the cosmological parameters that enter into our analysis are Ω_m^0 and parameters w_a and w_b which parametrise the equation of state of dark energy. We have obtained best-fit values of the parameters from analysis of the SNe Ia observational data. However, for a cosmographic analysis, which is a model independent way of processing cosmological data, the chosen parameter set is different. Basic aspects of cosmographic methodology and results of cosmographic analysis of SNe data are discussed in [82, 83, 84]. Here we briefly discuss the cosmography constructed from DE equation of state. We also qualitatively compare results of our analysis with the features of results of cosmographic analysis in terms of cosmographic parameters.

Neglecting the contribution to the present day energy density due to radiation Ω_r^0 in Eq. (4)

we can express the EOS parameter of dark energy as

$$\omega(z) = -1 + \frac{1}{3} \frac{[E(z)^2 - \Omega_m^0(1+z)^3]'(1+z)}{E(z)^2 - \Omega_m^0(1+z)^3} \quad (29)$$

where, ' in above equation denotes derivative with respect to z . We consider two cosmographic parameters: the deceleration parameter $q(z)$ and the jerk parameters $j(z)$ which are defined in a model independent way as

$$q(z) = -\frac{a\ddot{a}}{\dot{a}^2} \quad \text{and} \quad j(z) = \frac{\ddot{a}a^2}{\dot{a}^3} \quad (30)$$

These parameters are relevant in describing features of expansion of the universe. $q(z)$ is positive (negative) for a decelerating (accelerating) universe. Evolution of the jerk parameter $j(z)$ is relevant in search for departure from Λ -CDM model [85]. Exploiting the $d/dt = -(1+z)H(z)d/dz$ in above equations we in above equations we express $q(z)$ and $j(z)$ as

$$q(z) = -1 + \frac{1}{2}(1+z)\frac{[E(z)^2]'}{E(z)^2} \quad (31)$$

$$j(z) = \frac{1}{2}(1+z)^2\frac{[E(z)^2]''}{E(z)^2} - (1+z)\frac{[E(z)^2]'}{E(z)^2} + 1 \quad (32)$$

where ' in above two equations denote derivative with respect to z . Using Eq. (4) with $\Omega_r^0 = 0$ and $\Omega_{\text{de}}^0 = 1 - \Omega_m^0$ in Eqs. (31) and (32) and using expressions for $w(z)$ in terms of parameters w_a and w_b for different models considered in this work (as summarised in Tab. 1) we may express corresponding z -dependences of $q(z)$ and $j(z)$ involving parameters w_a , w_b and Ω_m^0 . Putting $z = 0$, we may then obtain relationships between w_a , w_b , Ω_m^0 , q_0 and j_0 , where q_0 and j_0 corresponds to the values of deceleration parameter and jerk parameter at present epoch. We may take these two parameters (q_0 and j_0) as cosmographic parameters relevant in this context. In the methodology of analysis described in Sec. 2, apart from the nuisance parameters α and β , the set (Ω_m^0, q_0, j_0) in stead of the set (Ω_m^0, w_a, w_b) may be chosen for a cosmographic analysis. A comprehensive statistical analysis of specific DE parametrisations using SNe Ia data have been performed in [82], which directly gives cosmographic parameters values. For a qualitative comparison, we have given in Tab. 4, the expressions for q_0 and j_0 for different DE parametrisations in terms of w_a , w_b and Ω_m^0 . As discussed in Sec. 4, for each of the varying dark energy Models, we obtained a point in $w_a - w_b$ parameter space (marked by P_1 in Fig. 3), corresponding to the parameters satisfying the physical bound $0 < c_s^2 < 1$. Values of these best-fits P_1 , are given in the last column of Tab. 2. For a comparison with the results of comprehensive cosmographic analysis performed in [82], we have also given in Tab. 4, the numerical values of q_0 and j_0 calculated using the their analytical expressions given in 2nd and 3rd column of the same table, at the point P_1 .

5 Conclusion

In this work we have performed a comprehensive analysis of recently released 'Joint Light-curve Analysis' (JLA) data to investigate its implications for models of dark energy with varying equation of state parameter $w(z)$. As a benchmark, we considered 4 different varying dark energy models, *viz.* CPL[25], JBP[29],[30], BA([31],[32]) and Logarithmic model [33],

Model	$q_0(w_a, \Omega_m^0)$	$j_0(w_a, w_b, \Omega_m^0)$	q_0 at P_1	j_0 at P_1
CPL	$\frac{(3w_a+1)\Omega_{de}^0+\Omega_m^0}{2(\Omega_{de}^0+\Omega_m^0)}$	$\frac{\Omega_{de}^0[3w_b+2+9w_a(w_a+1)]+2\Omega_m^0}{2(\Omega_{de}^0+\Omega_m^0)}$	-0.39	1.71
JBP		$\frac{\Omega_{de}^0[9w_a(w_a+1)+3w_b]+2\Omega_m^0}{2(\Omega_{de}^0+\Omega_m^0)}$	-0.08	1.96
BA		$\frac{3\Omega_{de}^0[w_b+3w_a(w_a+1)]+2\Omega_m^0}{2(\Omega_{de}^0+\Omega_m^0)}$	-0.52	0.58
Logarithmic		$\frac{\Omega_{de}^0[3w_a^2+3w_b-3w_a-4]+2\Omega_m^0}{2(\Omega_{de}^0+\Omega_m^0)}$	-0.47	1.36

Table 4: Expressions of cosmographic parameters q_0 and j_0 in terms of w_a, w_b, Ω_m^0 ($\Omega_{de}^0 = 1 - \Omega_m^0$) for different varying dark energy Models. Numerical values of q_0 and j_0 calculated using the expressions at point P_1 (see text for details) are also shown.

each of which involves a specific functional form of z -dependence of the dark energy equation of state $w(z)$. The analytical expression for the function $w(z)$ in each case involves two parameters, denoted by w_a and w_b . From the analysis of observational data we have obtained best-fit values of these parameters and also their ranges allowed at 1σ , 2σ and 3σ confidence level. Description of the data and methodology of analysis has been discussed in detail in Sec. 2. The results of the analysis are presented in table 2 and depicted in Fig. 3.

We make an attempt to realise the scenario of varying equation state of dark energy in terms of dynamics of a scalar field ϕ . We assume the scalar field to be homogeneous with its dynamics driven by a k -essence Lagrangian $L = VF(X)$, with a constant potential V and a dynamical term $F(X)$ with $X = (1/2)\nabla^\mu\phi\nabla_\mu\phi$. Consideration of constant potential ensures a scaling relation of the form $X(dF/dX)^2 = Ca^{-6}$ ($C = \text{constant}$) in FLRW spacetime background with scale factor a . We have exploited this to reconstruct functional form of $F(X)$ for the different varying dark energy models considered here (See Sec. 3 for details). The nature of $F(X)$ are obtained for each kind of $w(z)$ dependences corresponding to the best-fit parameters (w_a, w_b) . In this context, we also obtain the dependences of c_s^2 on z . c_s , as mentioned earlier, is the the speed with which small fluctuation in the background energy density grows. Stability of the density perturbations and causality requires c_s^2 to lie in the domain $0 < c_s^2 < 1$. The results show that at the best-fits, c_s^2 lies within its physical bound $0 < c_s^2 < 1$ only for a small range of values of z . For each of the varying DE models we have shown the region of the $w_a - w_b$ parameter space for which c_s^2 lies with its physical bound for all values of z accessible in SNe Ia observations. We finally find the point P_1 in $w_a - w_b$ parameter space for which $0 < c_s^2 < 1$ for all z and which is maximally favoured from the observational data. The z -dependence of c_s^2 and form of $F(X)$ are also obtained for this point (P_1) for all the varying DE models. These results are discussed in detail in Sec. 4 and depicted in Fig. 4. In this section we have also given a comparison of our results with those obtained from a comprehensive cosmographic analysis performed in [82].

6 Acknowledgments

We would like to thank the honourable referee for valuable suggestions. AC would like to thank University Grants Commission (UGC), India for supporting this work by means of

References

- [1] A. G. Riess *et al.* [Supernova Search Team], *Astron. J.* **116**, 1009 (1998) doi:10.1086/300499 [astro-ph/9805201].
- [2] S. Perlmutter *et al.* [Supernova Cosmology Project Collaboration], *Astrophys. J.* **517**, 565 (1999) doi:10.1086/307221 [astro-ph/9812133].
- [3] D. J. Eisenstein *et al.* [SDSS Collaboration], *Astrophys. J.* **633** (2005) 560 doi:10.1086/466512 [astro-ph/0501171].
- [4] Y. Zhang, arXiv:1411.5522 [astro-ph.CO]
- [5] E. Aubourg *et al.*, *Phys. Rev. D* **92**, no. 12, 123516 (2015) doi:10.1103/PhysRevD.92.123516 [arXiv:1411.1074 [astro-ph.CO]].
- [6] C. Blake and K. Glazebrook, *Astrophys. J.* **594**, 665 (2003) doi:10.1086/376983 [astro-ph/0301632].
- [7] H. J. Seo and D. J. Eisenstein, *Astrophys. J.* **598**, 720 (2003) doi:10.1086/379122 [astro-ph/0307460].
- [8] G. Hinshaw *et al.* [WMAP Collaboration], *Astrophys. J. Suppl.* **180**, 225 (2009) doi:10.1088/0067-0049/180/2/225 [arXiv:0803.0732 [astro-ph]].
- [9] E. Komatsu *et al.*, *Astrophys. J. Suppl.* 192, 18 (2011) doi: 10.1088/0067-0049/192/2/18 [arXiv:1001.4538[astro-ph]]
- [10] M. Tristram and K. Ganga, *Rept. Prog. Phys.* **70**, 899 (2007) doi:10.1088/0034-4885/70/6/R02 [arXiv:0708.1429 [astro-ph]].
- [11] E. Gawiser and J. Silk, *Phys. Rept.* **333**, 245 (2000) doi:10.1016/S0370-1573(00)00025-9 [astro-ph/0002044].
- [12] A. G. Riess *et al.*, *Astrophys. J.* **699**, 539 (2009) doi:10.1088/0004-637X/699/1/539 [arXiv:0905.0695[astro-ph]]
- [13] J. Simon, L. Verde and R. Jimenez, *Phys. Rev. D* **71**, 123001 (2005) doi:10.1103/PhysRevD.71.123001 [astro-ph/0412269].
- [14] E. Gaztanaga, A. Cabre, L. Hui, *Mon. Not. R. Astron. Soc.* **399**, 166 (2009) doi: 10.1111/j.1365-2966.2009.15085.x [arXiv:0902.1624[astro-ph]]
- [15] D. Stern, R. Jimenez, L. Verde, M. Kamionkauski, S. A. Stanford, *J. Cosmol. Astropart. Phys.* **1002**, 008 (2010) doi: 10.1088/1475-7516/2010/02/008 [arXiv:0907.3149[astro-ph]]
- [16] Y. Sofue and V. Rubin, *Ann. Rev. Astron. Astrophys.* **39**, 137 (2001) doi:10.1146/annurev.astro.39.1.137 [astro-ph/0010594].

- [17] D. Clowe, A. Gonzalez and M. Markevitch *Astrophys. J.* **604**, 596 (2004).
- [18] M. Bartelmann and P. Schneider, *Phys. Rept.* **340**, 291 (2001).
- [19] G. Hinshaw *et al.* [WMAP Collaboration], *Astrophys. J. Suppl.* **208**, 19 (2013).
- [20] P. A. R. Ade *et al.* [Planck Collaboration], *Astron. Astrophys.* **571**, A16 (2014).
- [21] S. Weinberg, *Rev. Mod. Phys.* **61**, 1 (1989)
- [22] Suzuki *et al.*, *ApJ* , **746** , 85 (2012) doi: 10.1088/0004-637X/746/1/85 [arXiv:1105.3470[astro-ph]]
- [23] M. Betoule *et al.* [SDSS Collaboration], *Astron. Astrophys.* **568**, A22 (2014) doi:10.1051/0004-6361/201423413
- [24] S. Wang, S. Wen and M. Li, *JCAP* **1703**, no. 03, 037 (2017) doi:10.1088/1475-7516/2017/03/037
- [25] Chevallier and Polarski, “Accelerating universes with scaling dark matter”, doi:10.1142/S0218271801000822”,
- [26] R. J. Scherrer, *Phys. Rev. D* **92**, no. 4, 043001 (2015) doi:10.1103/PhysRevD.92.043001 [arXiv:1505.05781 [astro-ph.CO]].
- [27] S. Linden and J. M. Virey, *Phys. Rev. D* **78**, 023526 (2008) doi:10.1103/PhysRevD.78.023526 [arXiv:0804.0389 [astro-ph]].
- [28] Dao-Jun Liu *et al.*, *Monthly Notices of the Royal Astronomical Society*, **388**, 21
- [29] H. K. Jassal, J. S. Bagla and T. Padmanabhan, *Mon. Not. Roy. Astron. Soc.* **356**, L11 (2005) doi:10.1111/j.1745-3933.2005.08577.x [astro-ph/0404378].
- [30] H. K. Jassal, J. S. Bagla and T. Padmanabhan, *Phys. Rev. D* **72**, 103503 (2005) doi:10.1103/PhysRevD.72.103503 [astro-ph/0506748].
- [31] E. M. Barboza, Jr. and J. S. Alcaniz, *JCAP* **1202**, 042 (2012) doi:10.1088/1475-7516/2012/02/042 [arXiv:1103.0257 [astro-ph.CO]].
- [32] E. M. Barboza, J. S. Alcaniz, Z.-H. Zhu and R. Silva, *Phys. Rev. D* **80**, 043521 (2009) doi:10.1103/PhysRevD.80.043521 [arXiv:0905.4052 [astro-ph.CO]].
- [33] A. Sangwan, A. Mukherjee and H. K. Jassal, *JCAP* **1801**, no. 01, 018 (2018) doi:10.1088/1475-7516/2018/01/018 [arXiv:1712.05143 [astro-ph.CO]].
- [34] C. Wetterich, *Phys. Lett. B* **594**, 17 (2004) doi:10.1016/j.physletb.2004.05.008 [astro-ph/0403289].
- [35] A. De Felice, S. Nesseris and S. Tsujikawa, *JCAP* **1205**, 029 (2012) doi:10.1088/1475-7516/2012/05/029 [arXiv:1203.6760 [astro-ph.CO]].
- [36] Y. Wang, *Phys. Rev. D* **77**, 123525 (2008) doi:10.1103/PhysRevD.77.123525 [arXiv:0803.4295 [astro-ph]].

- [37] M. Born and L. Infeld, Proc.Roy.Soc.Lond **A144**(1934) 425; C.Armendariz-Picon, T.Damour and V.Mukhanov, Phys.Lett. **B458** 209 (1999); C.Armendariz-Picon, V.Mukhanov and P.J.Steinhardt, Phys.Rev. **D63** 103510 (2001), Phys.Rev.Lett. **85** 4438 (2000); T. Chiba, T. Okabe and M. Yamaguchi, Phys.Rev.**D62** 023511 (2000); N. Arkani-Hamed, H. C. Cheng, M. A. Luty and S. Mukohyama, JHEP **05** (2004) 074, JCAP **0404** (2004) 001; R.R.Caldwell, Phys.Lett.**B545** (2002) 23
- [38] W. Heisenberg, Zeitschrift für Physik A, Hadrons and Nuclei **113** no. 1-2.
- [39] W. Heisenberg, Zeitschrift für Physik A, Hadrons and Nuclei **133** no. 1-2.
- [40] J. Q. Xia, Y. F. Cai, T. T. Qiu, G. B. Zhao and X. Zhang, Int. J. Mod. Phys. D **17**, 1229 (2008) doi:10.1142/S0218271808012784 [astro-ph/0703202].
- [41] E. Babichev, S. Ramazanov and A. Vikman, JCAP **1811**, no. 11, 023 (2018) doi:10.1088/1475-7516/2018/11/023 [arXiv:1807.10281 [gr-qc]].
- [42] A. Adams, N. Arkani-Hamed, S. Dubovsky, A. Nicolis and R. Rattazzi, JHEP **0610**, 014 (2006) doi:10.1088/1126-6708/2006/10/014 [hep-th/0602178].
- [43] E. Babichev, V. Mukhanov and A. Vikman, JHEP **0802**, 101 (2008) doi:10.1088/1126-6708/2008/02/101 [arXiv:0708.0561]
- [44] P. Astier *et al.* [SNLS Collaboration], Astron. Astrophys. **447**, 31 (2006) doi:10.1051/0004-6361:20054185 [astro-ph/0510447].
- [45] Sullivan *et al.*, ApJ, **737**, 102 (2011) doi:10.1088/0004-637X/737/2/102 [arXiv:1104.1444]
- [46] W. M. Wood-Vasey *et al.* [ESSENCE Collaboration], Astrophys. J. **666**, 694 (2007) doi:10.1086/518642 [astro-ph/0701041]
- [47] Tonry *et al.*, ApJ , **750** , 99 (2012) doi: 10.1088/0004-637X/750/2/99 [arXiv:1203.0297]
- [48] D. Scolnic *et al.*, Astrophys. J. **795**, no. 1, 45 (2014) doi:10.1088/0004-637X/795/1/45 [arXiv:1310.3824 [astro-ph.CO]].
- [49] Rest *et al.*, doi : 10.3847/2515-5172/aae371
- [50] W. Zheng, S. Y. Li, H. Li, J. Q. Xia, M. Li and T. Lu, JCAP **1408**, 030 (2014) Erratum: [JCAP **1409**, E01 (2014)] doi:10.1088/1475-7516/2014/09/E01, 10.1088/1475-7516/2014/08/030
- [51] J. A. Frieman *et al.*, Astron. J. **135**, 338 (2008) doi:10.1088/0004-6256/135/1/338 [arXiv:0708.2749 [astro-ph]].
- [52] Kessler *et al.*, ApJS , **185** , 32 (2009a) doi: 10.1088/0067-0049/185/1/32 [arXiv:0908.4274 [astro-ph]].
- [53] Sollerman *et al.*, ApJ , **703** ,1374 (2009) doi: 10.1088/0004-637X/703/2/1374 [arXiv:0908.4276 [astro-ph]].

- [54] Lampeitl *et al.*, MNRAS , **401** , 2331 (2010a) doi : 10.1111/j.1365-2966.2009.15851.x [arXiv:0910.2193 [astro-ph]].
- [55] Campbell *et al.*, ApJ , **763** ,88 (2013) doi: 10.1088/0004-637X/763/2/88 [arXiv:1211.4480 [astro-ph]].
- [56] Hicken *et al.*, ApJ , **700** , 331 (2009) doi: 10.1088/0004-637X/700/1/331 [arXiv:0901.4787 [astro-ph]].
- [57] Contreras *et al.*, AJ , **139** , 519 (2010) doi: 10.1088/0004-6256/139/2/519 [arXiv:0910.3330 [astro-ph]].
- [58] Folatelli *et al.*, AJ , **139** , 120 (2010) doi: 10.1088/0004-6256/139/1/120 [arXiv:0910.3317 [astro-ph]].
- [59] Stritzinger *et al.*, AJ , **142** , 156 (2011) doi: 10.1088/0004-6256/142/5/156 [arXiv:1108.3108 [astro-ph]].
- [60] M. Ganeshalingam, W. Li and A. V. Filippenko, Mon. Not. Roy. Astron. Soc. **433**, 2240 (2013) doi:10.1093/mnras/stt893 [arXiv:1307.0824 [astro-ph.CO]].
- [61] Aldering *et al.*, SPIE Conf. Ser , **4836** , 61
- [62] B. Leibundgut *et al.*, Astrophysical Journal Letters , **V 466** , 21; G. Goldhaber *et al.*, ApJ, **558** , 359; R. Foley *et al.*, ApJ, **626**, L11 ; I.M.Hook *et al.*, AJ, **130**, 2788; S. Blondin *et al.*, AJ, **131**, 1648; W.D.Li *et al.*, American Institute of Physics Conference Series, **103106** ; A.V. Filippenko *et al.*, ASP Conf. Ser. **332**; W. M. Wood-Vasey *et al.*, New Astronomy Review, **48** , 637; J. Frieman *et al.*, Bulletin of the American Astronomical Society, **1548**; B. Dilday *et al.*, Bulletin of the American Astronomical Society, **1459**; C. Lidman *et al.*, The Messenger, **118**, 24; M. Hamuy *et al.*, AJ, **112**, 2391 ; G. Miknaitis *et al.*, PASP, **53**, 224; T. Matheson *et al.*, AJ, **129**, 2352; W. Li *et al.*, PASP, **113**, 1178; W. Li *et al.*, PASP, **115**, 453; S. Jha *et al.*, AJ, **132**, 189; W.J. Percival *et al.*, MNRAS, **327**, 1297; G.M. Voit *et al.*, Reviews of Modern Physics, **77**, 207; E.V. Linder *et al.*, Physical Review Letters, **90**, 091301.
- [63] C. Hernandez-Monteagudo *et al.*, Mon. Not. Roy. Astron. Soc. **438**, no. 2, 1724 (2014) doi:10.1093/mnras/stt2312 [arXiv:1303.4302 [astro-ph.CO]]
- [64] J. Q. Xia, G. B. Zhao, B. Feng, H. Li and X. Zhang, Phys. Rev. D **73**, 063521 (2006) doi:10.1103/PhysRevD.73.063521 [astro-ph/0511625].
- [65] H. Li, Jun-Qing Xia, JCAP. **04** 026,(2010) doi:10.1088/1475-7516/2010/04/026 [arXiv:1004.2774 [astro-ph.CO]].
- [66] J. P. Dai, Y. Yang and J. Q. Xia, Astrophys. J. **857**, no. 1, 9 (2018). doi:10.3847/1538-4357/aab49a
- [67] W. Zheng, H. Li, J. Q. Xia, Y. P. Wan, S. Y. Li and M. Li, Int. J. Mod. Phys. D **23**, 1450051 (2014) doi:10.1142/S0218271814500515 [arXiv:1403.2571 [astro-ph.CO]].
- [68] J. Q. Xia, G. B. Zhao, H. Li, B. Feng and X. Zhang, Phys. Rev. D **74**, 083521 (2006) doi:10.1103/PhysRevD.74.083521 [astro-ph/0605366].

- [69] R. J. Scherrer, Phys. Rev. Lett. **93** 011301 (2004)
- [70] L. P. Chimento, Phys. Rev. **D69** 123517 (2004)
- [71] A. Vikman, K-essence: cosmology, causality and emergent geometry, Ph.D. thesis, Ludwig-Maximilians-Universitat, Munchen (2007)
- [72] Y. Aharonov, A. Komar, L. Susskind Phys Rev.**182.1400** doi : 10.1103/Phys-Rev.182.1400
- [73] C. Armendariz-Picon and E. A. Lim, JCAP **0508**, 007 (2005) doi:10.1088/1475-7516/2005/08/007 [astro-ph/0505207].
- [74] A. D. Rendall, Class. Quant. Grav. **23**, 1557 (2006) doi:10.1088/0264-9381/23/5/008 [gr-qc/0511158].
- [75] J. Garriga, V. Mukhanov, Phys. Lett. **B458** 219-225 (1999)
- [76] V.F.Mukhanov ,H.A.Feldman, R.H.Brandenberger Phys. Rept. 215 (1992) 203333.
- [77] V. Mukhanov, Physical foundations of cosmology. Cambridge, UK: Univ. Pr. (2005) 421
- [78] R. de Putter and E. V. Linder, Astropart. Phys. **28**, 263 (2007) doi:10.1016/j.astropartphys.2007.05.011 [arXiv:0705.0400 [astro-ph]].
- [79] L. R. Abramo and N. Pinto-Neto, Phys. Rev. D **73**, 063522 (2006) doi:10.1103/PhysRevD.73.063522 [astro-ph/0511562].
- [80] V. H. Crdenas, N. Cruz, S. Muoz and J. R. Villanueva, Eur. Phys. J. C **78**, no. 7, 591 (2018) doi:10.1140/epjc/s10052-018-6066-8 [arXiv:1804.02762 [gr-qc]].
- [81] W. H. Press, S. A. Teukolsky, W. T. Vetterling and B. P. Flannery, “Numerical Recipes in Fortran 77”, Cambridge University Press (1997)
- [82] C. Escamilla-Rivera and S. Capozziello, Int. J. Mod. Phys. D **28**, no. 12, 1950154 (2019) doi:10.1142/S0218271819501542 [arXiv:1905.04602 [gr-qc]].
- [83] S. Capozziello, R. D’Agostino and O. Luongo, Int. J. Mod. Phys. D **28**, no. 10, 1930016 (2019) doi:10.1142/S0218271819300167 [arXiv:1904.01427 [gr-qc]].
- [84] M. Benetti and S. Capozziello, arXiv:1910.09975 [astro-ph.CO].
- [85] A. Al Mamon and K. Bamba, Eur. Phys. J. C **78**, no. 10, 862 (2018) doi:10.1140/epjc/s10052-018-6355-2 [arXiv:1805.02854 [gr-qc]].